Integration of Different Solar Collectors into District Heating Networks and Floor Space Allocation

Maximilian Stahlhut[1], Cornelius Ackermann[1] and Thorsten Urbaneck[1]

[1] Chemnitz University of Technology, Department of Mechanical Engineering, Professorship Applied Thermodynamics, 09107 Chemnitz (Germany)

Abstract

For the direct integration of solar thermal systems into district heating networks many collectors with different design and thermal behavior are possible. This paper investigates four suitable collectors under different operating temperatures ($T_{DH,sup}$ = 95…140 °C) representing different generations of district heating networks. A flat-plate collector, a compound parabolic concentrator (CPC) collector and two parabolic trough collectors (PTC) were modeled in TRNSYS and simulated over a period of one year in three different scenarios and with different collector row distances. To determine a favorable collector, the heat production cost was calculated for the four collectors. The results show that in the investigated temperature range the CPC collector is the most suitable one. Depending on the defined scenario the CPC collector provides a specific annual yield (based on gross area) of 460…565 kWh m^{-2} a^{-1} with heat production cost of 33.41…40.85 € MWh^{-1}. This indicates that for most district heating applications the CPC collector is favorable.

Keywords: solar thermal, collector, field, shading, district heating, simulation, cost, floor space utilization

1. Introduction

Integration of collector fields into district heating (DH) networks is possible in various ways. A common variant is to build a solar secondary network. This integration is particularly recommended when planning new urban areas or developing neighborhood concepts, since the heating technology of the new buildings can be adapted to the lower temperatures of the solar local heating network. The low supply temperatures (e.g. $T_{DH,sup}$ = 75 °C in the solar local heating network in Chemnitz (Urbaneck et al., 2020) enable efficient use of flat-plate collectors (FPC). However, the construction of a suitable local heating network is not always feasible. In many cases, the solar heat must be fed into the existing network with supply temperatures varying from $T_{DH,sup}$ = 95…140 °C. Since heat supply with FPCs becomes increasingly inefficient at high temperature levels, these non-concentrating collectors are hardly used in district heating systems above 95 °C. For low and medium temperature ranges (100…150 °C) the stationary compound parabolic concentrator (CPC) collector and the parabolic trough collector (PTC) with single-axis tracking are suitable (Giovannetti and Horta, 2016). Both collectors have already been integrated in DH networks (Tian et al., 2018; Perers et al., 2013; Meißner and Moschke, 2016). Nonetheless, a comparison of the different solar collectors in terms of suitability for DH applications is not yet available. In this work a FPC, a CPC collector and two PTCs are modeled in the simulation software TRNSYS (Klein et al., 2017). Three scenarios are introduced which represent different operating conditions of the DH network. For comparing the collectors, they are simulated over the period of one year in three scenarios and with different floor space utilizations f_{col}. To determine a favorable collector and an optimal floor space utilization, the method of minimal heat production cost was applied.

2. Modeling in TRNSYS

2.1 Solar collectors

In this study, four commercially available collectors were modeled. The selection is intended to represent different collector setups which are suitable for low and medium operating temperatures. The modeling of the solar collectors includes one FPC *collector A)*, one CPC *collector B)* and two PTCs *collector C)* and *collector D)*. The two PTCs collector C) and collector D) differ by their concentration ratio *C*. *C* is the ratio of the aperture to the absorber surface. In principle, an increasing concentration ratio allows higher collector temperatures. Collector D) has a higher concentration ratio (*C* = 15) than collector C) (*C* = 8.5). The efficiency parameters of the collectors are summarized in Table 1. The quasi-dynamic collector model according to the European Standard EN 12975-2 (CEN, 2006) was

doi:10.18086/eurosun.2022.04.13 Available at http://proceedings.ises.org

used (Equation 1). The incidence angle modifier (IAM) for the beam radiation is summarized in the Appendix. The parameters a_3, a_4, a_5 and a_6 are not considered in the calculations (wind influence on heat losses, irradiance dependence on heat losses and thermal capacitance).

Tab. 1: TRNSYS Types for solar collectors and collector efficiency parameters based on gross area (K_d for collector B) is calculated in Type 71),

Collector	TRNSYS	η_0	a_1 [W m^{-2} K^{-1}]	a_2 [W m^{-2} K^{-2}]	K_d
A) FPC	Type 1289	0.763	1.971	0.015	0.873
B) CPC	Type 71	0.627	0.531	0.003	Type 71
C) PTC with C = 8.5	Type 1288	0.697	0.730	0.000	0.120
D) PTC with C = 15	Type 1288	0.717	0.107	0.001	0.000

$$\dot{q}_{\mathrm{col}} = \eta_0\left(K_{\mathrm{b}}G_{\mathrm{b,tilt}} + K_{\mathrm{d}}G_{\mathrm{d,tilt}}\right) - a_1(T_{\mathrm{m}} - T_{\mathrm{a}}) - a_2(T_{\mathrm{m}} - T_{\mathrm{a}})^2 \qquad \text{(eq. 1)}$$

The stationary collectors collector A) and collector B) are positioned with an azimuth of γ_{col} = 180° and a surface tilt of β = 35°. The two PTCs collector C) and collector D) are operated with a continuous single-axis tracking to reduce the incident angle Θ,i on the collector surface. In principle, a distinction can be made between two tracking variants for single-axis tracking:

- alignment of the collector axis in north-south direction (N-S) with a continuous tracking from east to west,
- alignment of the collector axis in east-west direction (E-W) with a continuous change of the surface tilt.

By changing the tracking angle β with the position of the sun, the angle of incidence in the transverse plane to the absorber tube is continuously zero degrees. An angular deviation is only perceivable in the longitudinal plane.

A deviation from the optimal angle of incidence Θ,i = 0° leads to a lower usable radiation fraction and thus to so-called cosine losses. The cosine losses result from a non-optimal angle of incidence of the beam radiation on the collector surface, whereby the relationship according to Equation 2 applies.

$$G_{\mathrm{b,tilt}} = G_{\mathrm{b},\Theta,\mathrm{i}=0°} \cdot cos\Theta,\mathrm{i} \qquad \text{(eq. 2)}$$

Figure 1 shows the beam irradiation for the collectors with a fixed surface tilt of β = 35° and for the PTCs with a continuous single-axis tracking in N-S and E-W alignment. Figure 1 further provides the direct normal irradiation (DNI). DNI is the amount of solar radiation received if the collector plane is always held perpendicular to the solar beam rays (no cosine losses). It can be seen that the tracking increases the amount of usable beam irradiation. The N-S orientation has advantages in the summer period, while the E-W orientation can use more beam irradiation in winter. For Chemnitz (Germany) the N-S orientation is preferable due to lower cosine losses. Therefore, this orientation is favored in the further study.

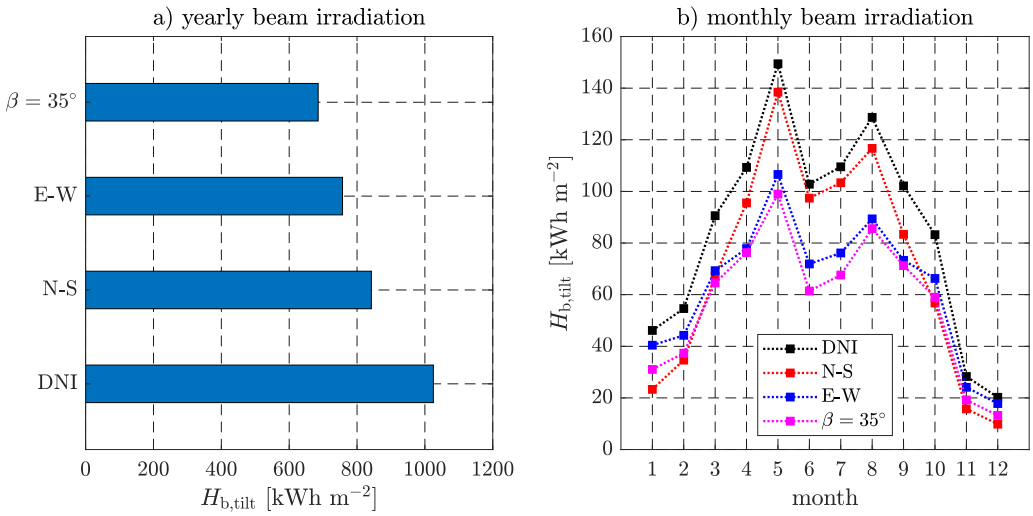

Fig. 1: Yearly and monthly beam irradiation for a fixed surface tilt of β = 35° and γ_{col} = 180°, continuous tracking with E-W alignment, continuous tracking with N-S alignment and DNI

2.2 Collector array shading

An essential aspect in the planning of a collector field is the consideration of collector array shading. These shading losses vary with the altitude and the azimuth of the sun and are significantly influenced by the collector tilt and the floor space utilization f_{col}. The floor space utilization is defined by the ratio between the distance of two collector rows and the collector length. It indicates how much of the field area is used by the solar collectors. As f_{col} increases, the distance between the collector rows decreases and the losses due to shading rise.

Figure 2 shows the losses due to row shading (exemplary for October 21) for different floor space utilizations for non-tracking ($\beta = 35°$) and single-axis tracking collectors with N-S alignment. The calculations were performed using TRNSYS and the Type 30 (TRNSYS model) for the non-tracking collectors A) and B), and using the Type 1262 for the tracking collectors C) and D) with N-S alignment. It can be seen that the shading curves differ significantly.

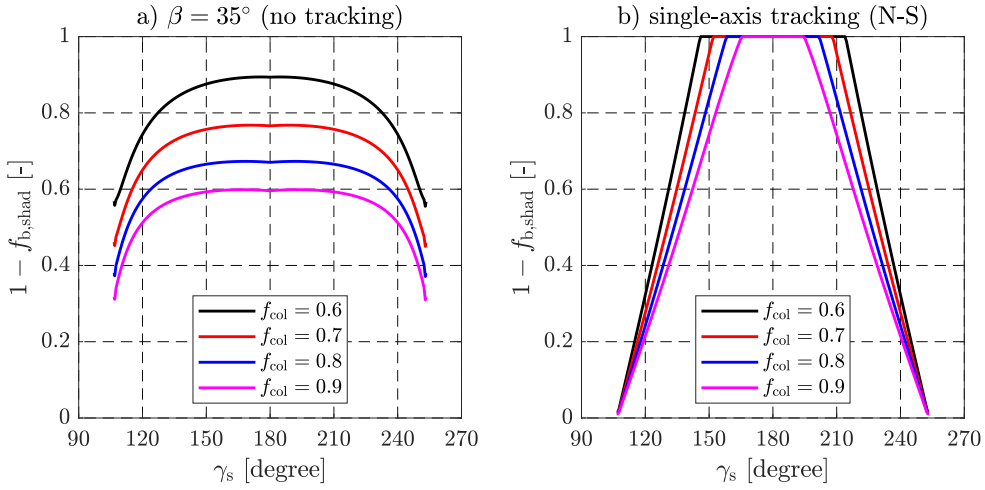

Fig. 2: Influence of collector array shading on October 21 for a) non-tracking collectors with $\beta = 35°$ and $\gamma_{col} = 180°$ and b) single-axis tracking with N-S alignment

In the morning and evening hours, the relative shading losses $f_{b,shad}$ dominate for the tracking collectors C) and D). At maximum solar elevation, no shading losses occur for the tracking collectors regardless of the floor space utilization. At this time of the day the tracking collectors are in a horizontal position. In the case of the collectors A) and B) with a fixed slope, shading losses can also occur at midday, depending on the elevation of the sun and the distance between the collector rows.

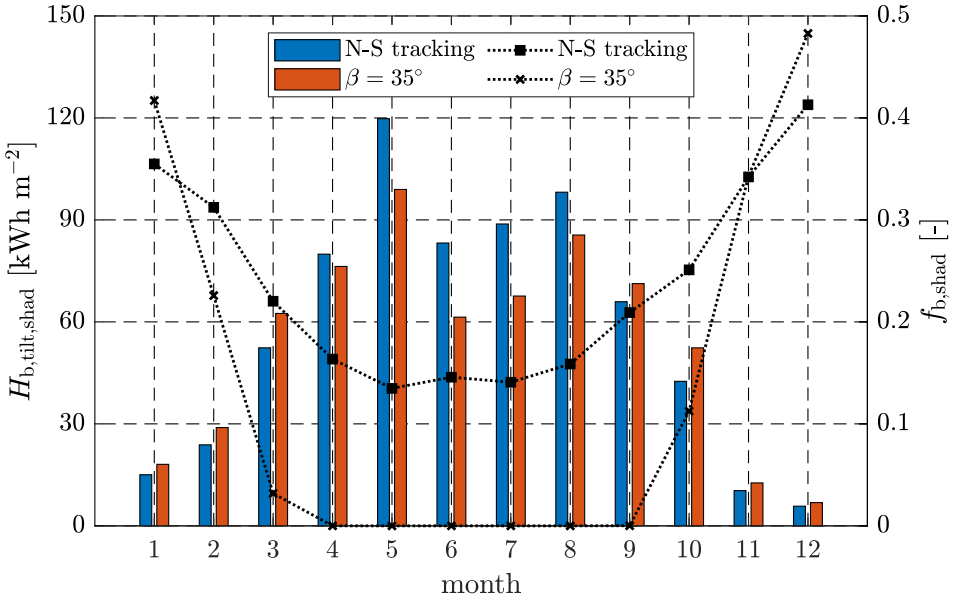

Fig. 3: Beam irradiation subtracted by shading losses for non-tracking ($\beta = 35°$ and $\gamma_{col} = 180°$) and tracking collectors (N-S) for $f_{col} = 0.6$

Figure 3 shows the beam irradiation subtracted by the shading losses for the non-tracking and tracking collectors for $f_{col} = 0.6$. In the summer months the collectors C) and D) cannot use 10…20 % of the beam irradiation due to shading losses. For the collectors A) and B) only a small amount of shading occurs in the months March to September. In total, 6% of the annual beam irradiation is shaded for collectors A) and B) and 18% for collectors C) and D). Figure 4 illustrates the reason for the higher shading losses. Despite the greater shading losses for the two PTCs, the usable beam irradiation is greater than for the non-tracking collectors due to fewer cosine losses.

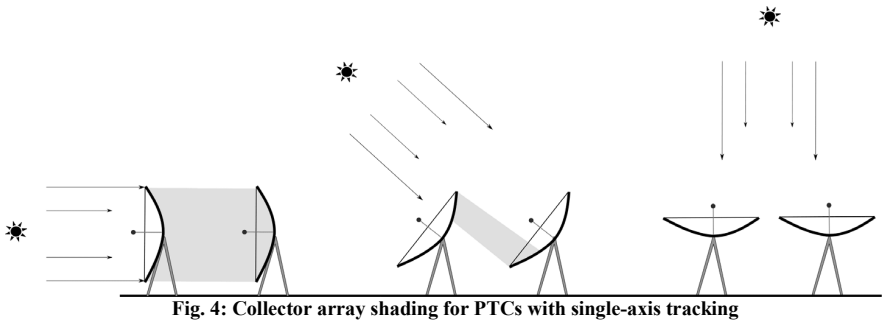

Fig. 4: Collector array shading for PTCs with single-axis tracking

2.3 District heating network

The four collectors were modeled in the simulation program TRNSYS in a system according to Figure 5. The heat transfer medium is taken from the return line of the DH network and heated by the solar system and then fed into the supply line of the DH network. The outlet temperature of the collector is set, so that the supply temperature of the DH network is reached. If the outlet temperature is too small, the three-way valve TWV1 is in position 2 and the collector fluid is preheated.

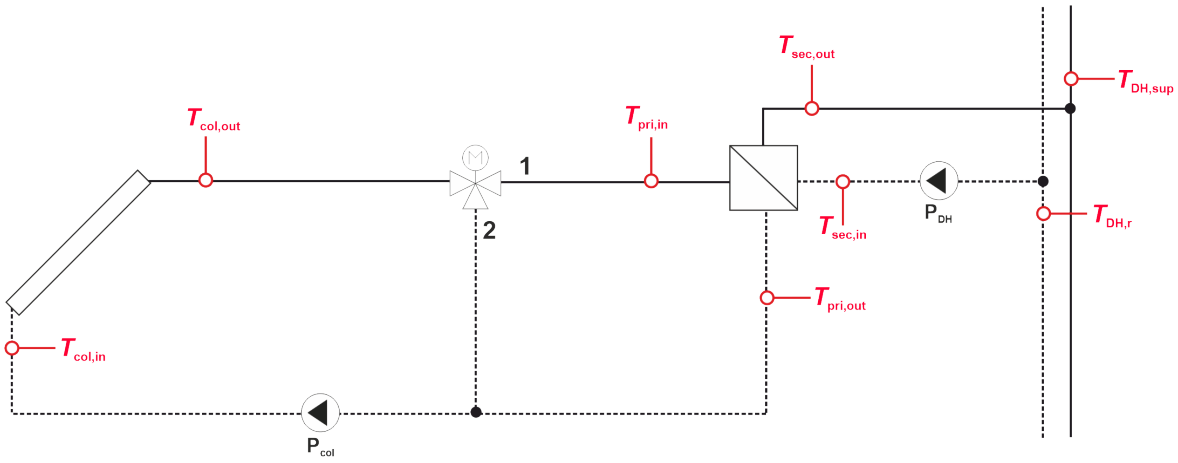

Fig. 5: Hydraulic scheme for solar collectors with direct integration in the DH network

The system in Figure 5 was simulated over a period of one year. Two weather data sets (test reference year, TRY) for Chemnitz (Germany) are used within the scope of this study: current TRY (2015) and a forecast TRY (2045). Both data sets were obtained by the online databank of the DWD (2021). The ambient temperature as well as the irradiation in the weather dataset for the year 2045 is slightly increased compared to the current weather data set. Furthermore, the proportion of the yearly beam irradiation is higher in TRY 2045. This weather dataset intends to map the impact of climate change.

For considering different operating temperatures of the DH system three scenarios are introduced:

Scenario 1 assumes an operation with a continuous adjustment of the supply temperature according to the outdoor temperature:

- $T_{DH,sup} = 110$ °C if $T_a < -10$ °C and $T_{DH,sup} = 95$ °C if $T_a \geq 15$ °C, in between linear interpolation
- $T_{DH,r} = 55$°C = constant

This is a possible future scenario, which is why the weather data set for the year 2045 was used for the simulation. In this scenario, the supply and return temperatures of the DH networks are the lowest compared to the other scenarios.

In *Scenario 2*, there is a monthly adjustment of the supply and return temperature:

- January to March and October to December $T_{DH,sup}$ = 120 °C and $T_{DH,r}$ = 62 °C
- April to December $T_{DH,sup}$ = 100 °C and $T_{DH,r}$ = 70 °C

This scenario reflects a typical contemporary grid operation with relatively low temperatures. The current weather data set is used.

Scenario 3 also uses a monthly adjustment of the supply and return temperatures:

- January to March and October to December $T_{DH,sup}$ = 140 °C and $T_{DH,r}$ = 65 °C
- April to December $T_{DH,sup}$ = 120 °C and $T_{DH,r}$ = 70 °C

However, higher grid temperatures are assumed. Since this is a representation of the current situation, the simulation also uses the current weather data set.

2.4 Heat production cost

For the selection of an optimal floor space utilization, a simplified economic evaluation is carried out on the basis of minimum heat production costs with the annuity method according to VDI 2067 (VDI, 2012). A technical utilization period of the entire plant of 25 years and an interest rate of 1 percent per year are assumed. The demand-related costs refer to the electricity consumption of the pumps and take into account an electricity price of k_{el} = 0.30 € kWh^{-1}. The operation-related costs can arise, among other things, from maintenance and servicing of the system. The operation-related costs are given in VDI 6002 (VDI, 2014) as approximately 1 percent of the investment costs. For the two parabolic trough collectors, the annual operating costs are estimated at about 3 percent of the investment costs. Due to the tracking as well as a possible cleaning of the reflectors, the operating costs assumed higher for this collector design.

The investment costs (excluding the costs for collectors) are supposed to be equal for all collector technologies with K_{Inv} = 10,685,000 €. The collector-specific costs are based on the following values:

$$k_{\mathrm{col}} = \begin{cases} 211\,\frac{€}{m^2} \cdot A_{\mathrm{collector\ A)}} \\ 223\,\frac{€}{m^2} \cdot A_{\mathrm{collector\ B)}} \\ 350\,\frac{€}{m^2} \cdot A_{\mathrm{collector\ C)}} \\ 350\,\frac{€}{m^2} \cdot A_{\mathrm{collector\ D)}} \end{cases} \qquad \text{(eq. 3)}$$

3. Results

An increase in the floor space utilization f_{col} increases the collector's annual yield. At the same time, the shading losses increase with decreasing row spacing, so that the annual yield does not increase linearly with f_{col}. Figure 6 illustrates the annual yield for the four collectors at f_{col} = 0.4…0.9 and the defined scenarios for a field area of approximately 98,525 m^2 (Mücke et al., 2021). It can be seen that collector B) provides the most annual yield in all three scenarios independent of the floor space utilization. Looking at the curve shapes of all four collectors, it is noticeable that the two PTCs, collector C) and collector D) have a flatter curve than collector B). This can be attributed to a greater increase in shading losses for the collectors with single-axis tracking. Collector A) (flat-plate collector) has a similar curve as collector B) in scenario 1. Up to a floor space utilization of f_{col} = 0.7, the curve is almost linear and then it starts to flatten. In scenario 2 and scenario 3 (at a higher temperature level) the flattening of the curve begins earlier for collector A). Collector B) has the steepest curve in comparison to the other collectors. Rising f_{col} increases the annual yield the most for this collector. The yield differences of the two PTCs collector C) and collector D) are marginal.

Figure 7 shows the heat production cost for the four collectors for different degrees of floor space utilization f_{col} as well as the defined scenarios. It can be seen that collector B) has the lowest cost in all three scenarios independent of f_{col}. The heat production costs of the CPC collector are almost half less than for the two PTCs, collector C) and collector D). In Scenario 1 collector A) has lower heat production cost in comparison to the collectors C) and D) at f_{col} = 0.4 and f_{col} = 0.5. In scenario 2 and scenario 3, collector A) has the highest heat production cost at all floor space utilizations. The lower investment cost cannot compensate for the low annual yield.

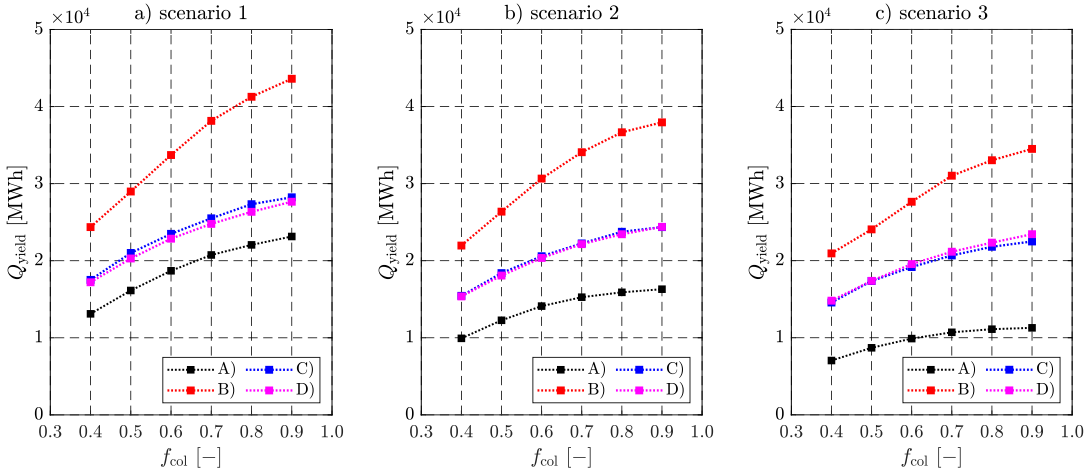

Fig. 6: Annual yield for the collectors A), B), C) and D) for different f_{col} and scenarios for a field area of 98,525 m²

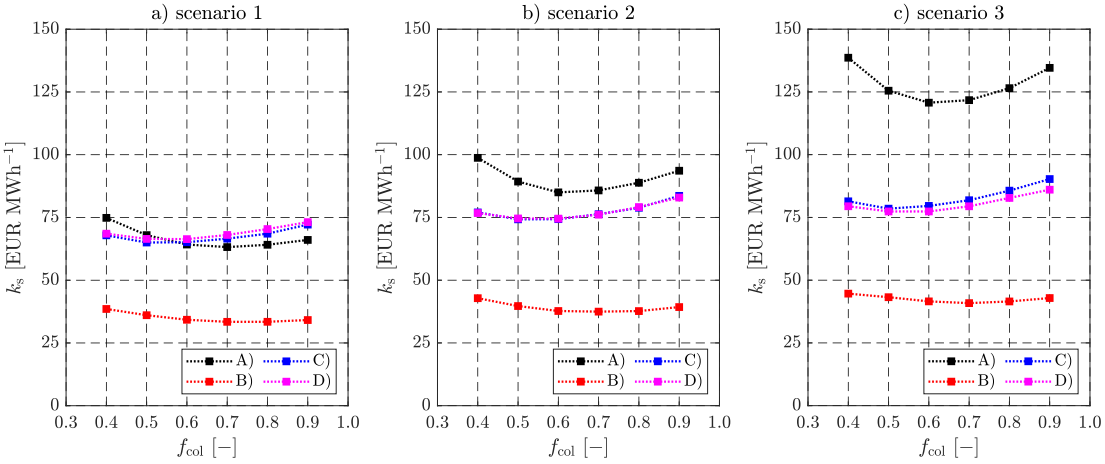

Fig. 7: Heat production cost k_s for the collectors A), B), C) and D) for different f_{col} and scenarios

Tab. 2: Floor space utilization f_{col} and specific annual yield q_{yield} (based on gross collector area) at minimum heat production cost for the collectors A), B), C), D) and for the different scenarios

scenario	f_{col}	k_s [€ MWh^{-1}]	q_{yield} [kWh m^{-2}a^{-1}]
collector A) – flat-plate collector			
scenario 1	0.7	63.14	310
scenario 2	0.6	84.92	246
scenario 3	0.6	120.62	172
collector B) – CPC collector			
scenario 1	0.7	33.41	565
scenario 2	0.7	37.47	505
scenario 3	0.7	40.85	460
collector C) – PTC C = 8,5			
scenario 1	0.5	65.01	430
scenario 2	0.5	74.24	377
scenario 3	0.5	78.48	356
collector D) – PTC C = 15			
scenario 1	0.6	66.36	399
scenario 2	0.6	74.52	355
scenario 3	0.6	77.37	341

Figure 7 also displays that the optimal floor space utilization f_{col} differs between the collectors. The PTC tends to have a minimum of k_s at a smaller floor space utilization than the CPC. This can be explained with higher shading losses for the PTC due to the tracking mechanism. At an optimum floor space utilization of f_{col} = 0.7 the collector B) has k_s of 33.41 € MWh^{-1} for scenario 1, 37.45 € MWh^{-1} for scenario 2 and 40.85 € MWh^{-1} for scenario 3. The specific annual yield (based on gross area) for collector B) in scenario 1 is 565 kWh m^{-2} a^{-1}, in scenario 2 505 kWh m^{-2} a^{-1} and in scenario 3 460 kWh m^{-2} a^{-1}. Increasing the floor space utilization to f_{col} = 0.9 increases the annual yield Q_{yield} about 11.2% - 14.3% while decreasing k_s about 2.1% - 5.0%.

4. Discussion

The results of the investigation show that collector B) (CPC collector) provides the most yield in the three defined scenarios and thus in the temperature range of $T_{DH,sup}$ = 95...140 °C at the floor space utilizations f_{col} = 0.4...0.9. Moreover, the heat production cost of collector B) is the lowest at all floor space utilizations. The minimum heat production costs result at f_{col} = 0.7 with k_s = 33.41...40.85 € MWh^{-1}. When comparing collector B) with the two PTCs, collector C) and collector D), it becomes clear that due to greater shading losses, the optimal floor space utilization for the PTCs is lower than that of the CPC collector. Thus, the single-axis tracking collectors use the total collector field area less efficient.

Although single-axis tracking increases the usable fraction of beam radiation by reducing cosine losses, collector C) and collector D) provide less annual yield than the non-tracking collector B). This can be mainly attributed to the fact that at the investigation area (Chemnitz, Germany) about 52% of the annual global irradiation is diffuse. Due to the relatively large concentration ratio of the parabolic trough collectors, only a small part of the diffuse radiation arriving from a wide angular range can be utilized for heat generation.

The results of the study confirm that the direct integration of solar systems into district heating networks is efficiently possible without the construction of a secondary network. For an efficient use of the solar heat it should be integrated in the district heating network in such a way that largest possible coverage of the district heating load is achieved by the solar system in the summer period.

5. Acknowledgments

The authors would like to thank *inetz* for providing and allowing the use of information. Special thanks also go to the Chemnitz city administration for commissioning and cooperating in the project "*Erstellung eines Klimaschutzteilkonzeptes für die Stadt Chemnitz zur Erschließung der Potenziale regenerativer Energien im Hinblick auf die CO_2-Reduktionsziele 2050*."

6. References

CEN European committee for standardization, 2006. EN 12975-2:2006 Thermal solar systems and components – Collectors – Part 2: Test methods.

Deutscher Wetterdienst, 2021. Testreferenzjahr Standort Chemnitz, https://www.dwd.de (last accessed on 10.03.22).

Giovannetti, F., Horta, P., 2016. Comparison of process heat collectors with respect to technical and economical conditions. International Energy Agency, Solar Heating & Cooling Programme, Task 49.

Klein, S. A. et al., 2017. TRNSYS 18: A Transient System Simulation Program. Solar Energy Laboratory, University of Wisconsin, Madison, USA, http://sel.me.wisc.edu/trnsys.

Meißner, R., Moschke, D., 2016. Senftenberg – Ergebnisse des ersten Betriebsjahres. https://www.ritter-xl-solar.de/senftenberg-ergebnisse-des-ersten-betriebsjahres/ (last accessed on 10.03.22).

Mücke, J. M., Böhme, H., Urbaneck, T., 2021. Klimaschutzteilkonzept Stadt Chemnitz - Erschließung der Potenziale regenerativer Energien im Hinblick auf die CO_2-Reduzierungsziele 2050. Abschlussbericht, www.chemnitz.de 17.03.2021. – ISBN 987-3-9812586-6-0

Perers, B., Furbo, S., Dragsted, J., 2013. Thermal performance of concentrating tracking solar collectors. Technical University of Denmark, Department of Civil Engineering. DTU Civil Engineering Reports No. R-292

Tian, Z., Perers, B., Furbo, S., Fan, J., 2018. Thermo-economic optimization of a hybrid solar district heating plant

with flat plate collectors and parabolic trough collectors in series. Energy Conversion and Management. 92-101. – ISSN 0196-8904 https://doi.org/10.1016/j.enconman.2018.03.034.

Urbaneck, T.; Shrestha, N. Lal; Oppelt, T.; Frotscher, O.; Göschel, T.; Uhlig, U.; Frey, H., 2020. Solare Fernwärme für das Quartier Brühl in Chemnitz – Begleitforschung (SolFW). Technische Universität Chemnitz, Fakultät für Maschinenbau, Professur Technische Thermodynamik (Ed.), inetz GmbH (Ed.) - ISBN: 987-3-9812586-5-3, Open Access: https://nbn-resolving.org/urn:nbn:de:bsz:ch1-qucosa2-390452

VDI Verein deutscher Ingenieure, 2012. VDI 2067 Part 1 Economic efficiency of building installations – Fundamentals and economic calculation.

VDI Verein deutscher Ingenieure, 2014. VDI 6002 Part 1 Solar heating in portable water – Basic principles – System technology and application in residential buildings.

Abbreviations

Quantity	Symbol
Compound parabolic concentrator	CPC
Deutscher Wetterdienst	DWD
Direct normal irradiation	DNI
District heating	DH
East-West alignment	E-W
Flat-plate collector	FPC
Incidence angle modifier	IAM
North-South alignment	N-S
Parabolic trough collector	PTC
Pump	P
Test reference year	TRY
Three way valve	TWV

Symbols

Quantities

Quantity	Symbol	Unit
Area	A	m^{-2}
Heat loss coefficient at $(T_m-T_a) = 0$	a_1	W m^{-2} K^{-1}
Temperature dependence of the heat loss coefficient	a_2	W m^{-2} K^{-2}
Concentration ratio	C	
Factor	f	
Floor space utilization	f_{col}	
Beam irradiance	G_b	W m^{-2}
Diffuse irradiance	G_d	W m^{-2}
Beam irradiation	H_b	kWh m^{-2}
Diffuse irradiation	H_d	kWh m^{-2}
Incidence angle modifier	K	
Electric cost	k_{el}	€ kWh^{-1}
Investment cost	K_{Inv}	€
Heat production cost	k_s	€ MWh^{-1}
Heat quantity	Q	MWh
Specific heat quantity	q	kWh m^{-2}
specific Heat	$\dot{q}$	W m^{-2}
Temperature	T	°C
Surface tilt	β	0 to ± 90°; toward the equator is +ive
Azimuth (of surface)	γ	0 to 360°; clockwise from North is +ive
Incidence (on surface)	Θ,i	0 to + 90°
Longitudinal incidence angle	Θ,L	0 to + 90°
Transversal incidence angle	Θ,T	0 to + 90°
Zero loss efficiency	η_0	

Subscripts

Quantity	Symbol
Ambient	a
Beam	b
Collector	col
Diffuse	d
District heating	DH
Electric	el
Incidence	i
Investment	Inv
Mean	m
Primary	pri
Return	r
Solar	s
Secondary	sec
Shading	shad
Supply	sup
Tilted surface	tilt

Appendix: INCIDENCE ANGLE MODIFIER FOR BEAM RADIATION

Tab. 1: IAM beam radiation for collector A)

Θ_i	0°	10°	20°	30°	40°	50°	60°	70°	80°	90°
K_b	1.00	1.00	0.99	0.98	0.96	0.91	0.82	0.53	0.27	0.00

Tab. 2: IAM beam radiation for collector B)

Θ_L , Θ_T	0°	10°	20°	30°	40°	50°	60°	70°	80°	90°
$K_b(\Theta_L)$	1.00	1.00	0.99	0.96	0.93	0.9	0.87	0.86	0.43	0.00
$K_b(\Theta_T)$	1.00	1.02	1.03	1.03	1.03	0.96	1.07	1.19	0.60	0.00

Tab. 3: IAM beam radiation for collector C)

Θ_L , Θ_T	0°	10°	20°	30°	40°	50°	60°	70°	80°	90°
$K_b(\Theta_L)$	1.00	0.99	0.99	0.98	0.96	0.91	0.77	0.53	0.18	0.00
$K_b(\Theta_T)$	1.00	1.00	1.00	1.00	1.00	1.00	1.00	1.00	1.00	0.00

Tab. 4: IAM beam radiation for collector D)

Θ_L , Θ_T	0°	10°	20°	30°	40°	50°	60°	70°	80°	90°
$K_b(\Theta_L)$	1.00	0.95	0.92	0.88	0.82	0.71	0.55	0.31	0.00	0.00
$K_b(\Theta_T)$	1.00	1.00	1.00	1.00	1.00	1.00	1.00	1.00	1.00	0.00